COMMUNICATION

Orientation of a Helical Nanofilament (B4) Liquid-Crystal Phase: Topographic Control of Confinement, Shear Flow, and Temperature Gradients

*Dong Ki Yoon, Youngwoo Yi, Yongqiang Shen, Eva D. Korblova, David M. Walba, Ivan I. Smalyukh, and Noel A. Clark**

The liquid-crystal (LC) phases of bent-core molecules have been of great interest because of their unusual polar and chiral properties, as well as their exotic collective behavior, including the formation of macroscopic chiral structures from achiral molecules.[1–9] The bent-core molecules strongly nanosegregate, leading to the formation of polar and chiral arrangements of the bent cores into planar or modulated layers. Subtle interactions between layers can be manipulated to produce a variety of ferro- or anti-ferroelectric phases.

Among the most mysterious and interesting of these new phases is the B4, a locally layered phase with hexatic or semicrystalline ordering of the layers, showing large optical rotation and light scattering which suggests a strongly chiral local structure. Recently, it has been shown that the B4 is a phase of spontaneously self-assembling helical nanofilaments (HNFs), the morphology of which is driven by a tendency for local saddle splay deformation of the semicrystalline layers.[7] These nanofilaments, shown in **Figure 1**b for the bent-core material NOBOW (benzoic acid, 4-[(E)-([4-(nonyloxy)phenyl]imino) methyl]-,1,1'-(1,3-phenylene)ester) (Figure 1a) grow from the higher temperature isotropic or fluid bent-core phases with a well-defined pitch of the helical twist and lateral structure and dimensions. The bulk B4 is a close packing of HNFs in which the filament axes are parallel to one another and their layer twist becomes macroscopically coherent. In the filament growth process a nucleation event establishes the handedness of a filament and this handedness is transferred to subsequently growing filaments to form large (≈100-μm dimension) homochiral domains with either right-handed and left-handed characteristics. Atomic force microscopy (AFM) imaging of the air/LC surface of the B4 reveals this bulk structure, showing clearly the collective ordering of the HNF helices (Figure 1c).[7]

Bent-core mesogens such as NOBOW are low-molecular-weight liquid-crystalline materials that can include molecular design features that give specific properties and functionalities, for example large, second order, nonlinear optical susceptibilities or electrical conductivity. In such cases the chiral nanofilament superstructures can offer intriguing possibilities for the production of novel materials. Achieving alignment thus opens a wide variety of opportunities for the production of functional chiral materials for application in organic semiconductors, thin-film polarizers, thin-film transistors, lasers, and solar cells via controlled self-organization of bent-core molecules.[10–14]

Currently available evidence indicates that it is difficult to achieve macroscopically oriented domains of the B4 phase. The B4 grows from the higher temperature fluid smectic or isotropic phase via a first-order phase transition in which nanofilament formation starts at dilute nucleation sites. Growth from a texture of B2 focal conic domains yields a B4 texture with similar focal conic patterns but much lower birefringence, Δn, which indicates either a weak control of the B4 growth process by the existing fluid smectic layering, or that the B4 just has low Δn.[15] Growth of the B4 from the isotropic phase, for example in mixtures of NOBOW and calamitic LCs, is in the form of flower-like spherulites with the filaments generally radial but highly disordered.[16,17] Shearing of NOBOW between glass plates increases the birefringence Δn of its fluid smectic B2 and B3 phases by ten times relative to that of an unsheared filled cell, producing nearly complete alignment these phases, but increases the birefringence of the B4 only by two times, to $\Delta n \approx 0.04$, to about 25% of that of the B2.[23] It is not clear whether this low measured value is due to low inherent Δn or poor alignment.

Here, orientational control of HNF growth is reported. Initial efforts using the topographic surface patterning techniques that have proven successful in the orientation of nematic and smectic phases of calamitic LCs were not successful.[18] However, it was found that such topographical confinement can combine with the thermal confinement and shear-induced orientation produced by air flow over the surface to align HNFs. HNF alignment was directly investigated by various microscopic techniques including depolarized transmitted light microscopy (DTLM), depolarized reflected light microscopy (DRLM), scanning electron microscopy (SEM), and AFM. Just as alignment control has been the key to the development of all known applications of LCs, such as their various display modes, controlling

Dr. D. K. Yoon, Dr. Y. Yi, Y. Shen, Prof. I. I. Smalyukh, Prof. N. A. Clark
Department of Physics and Liquid Crystal Materials Research Center
University of Colorado
Boulder, CO 80309-0390, USA
E-mail: noel.clark@colorado.edu
Dr. E. D. Korblova, Prof. D. M. Walba
Department of Chemistry and Liquid Crystal Materials Research Center
University of Colorado
Boulder, CO 80309-0215, USA
Prof. I. I. Smalyukh
Renewable and Sustainable Energy Institute
University of Colorado
Boulder, CO 80309, USA

DOI: 10.1002/adma.201004482

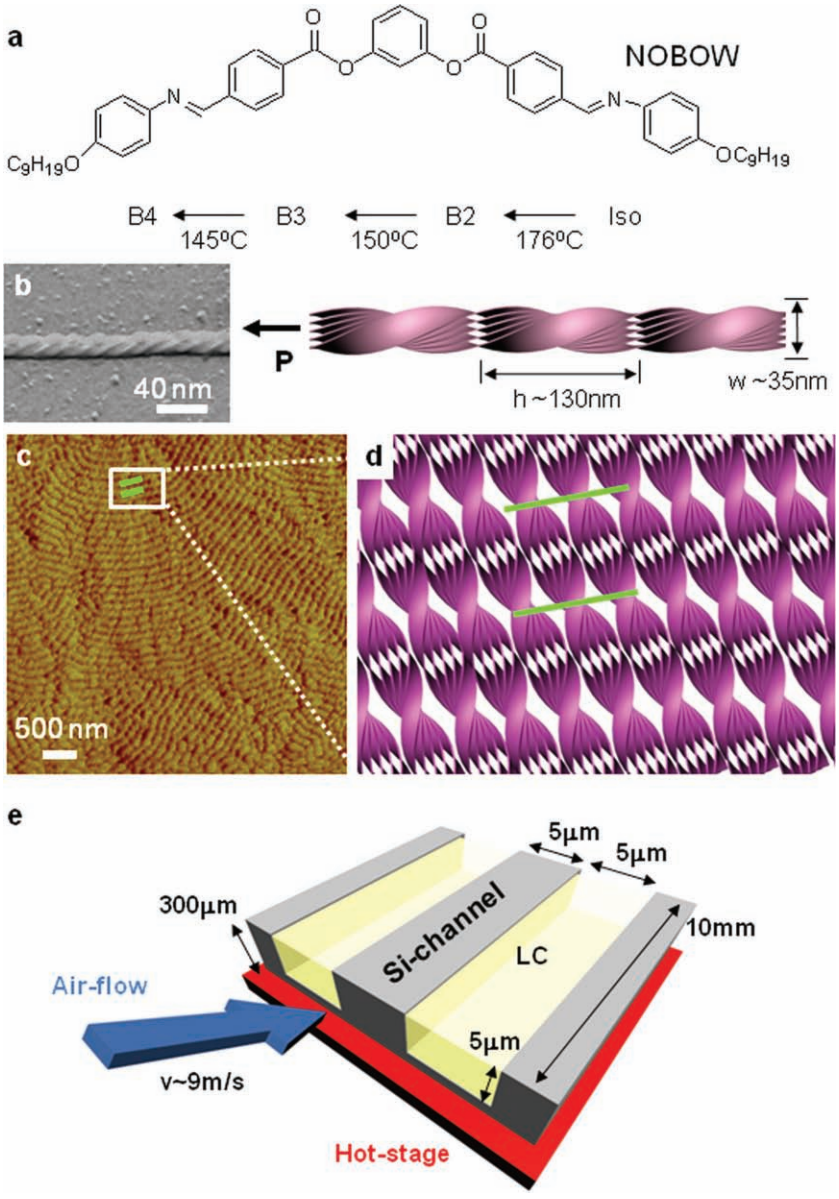

Figure 1. Material, molecular ordering scheme, and experimental setup. a) The molecular structure and phase sequence upon cooling from isotropic phase. b) The nanofilament phase is composed of well-defined smectic layers, revealing macroscopic polarization and tilt of these layers, making this structure chiral, including mesogenic units (bent-cores) in the layers. Width (w) and half pitch (h) of single filament are $w \approx 35$ m and $h \approx 30$ nm, and P is the director of HNFs. c) An AFM image of HNFs shows line patterns in which the gap between green lines is the half pitch ($h \approx 130$ nm) of HNFs. d) Schematic of (c) shows how HNFs are aligned. e) In order to apply a confining effect on the HNFs, NOBOW is filled in the isotropic phase by capillarity into channels of 5-µm-depth, 5-µm-width, and 10-mm-length etched into the surface of a Si wafer. Air flow (velocity, $v \approx 9$ m s^{-1}) was then supplied through a pipe of 4-mm-inner-diameter at an angle of 30° from the surface upon cooling from the isotropic to the B4. The air flow was used to generate flow of the B4 to control the orientation of the HNFs.

HNF orientation promises important ways to use their chiral superstructures in soft materials as the cornerstone of new applications. The use of topographic confinement is used not only to directly control LC alignment, but also to provide control of LC temperature and flow characteristics operative in the alignment process.

Upon cooling from the isotropic phase NOBOW forms the B2, a fluid smectic phase with spontaneously polar ordering of the bent cores in the layers and tilt of the molecular planes from the layer normal.[1,4] The B2 layers preferentially orient normal to the Si wafer/LC and glass/LC interfaces and parallel to the LC/air interface (Supporting Information, Figures S1–S3). These orientations are evidenced by the appearance of toroidal focal conic defects in thin films on flat glass or Si and in the 10-µm-width channel (Supporting Information, Figure S4).[18] Upon the transition to the B3 phase some degree of in-plane hexatic ordering appears, but the layer textures do not change. The transition to the B4 phase is strongly first order, with the development of more crystal-like in-plane ordering and a substantial decrease in the layer spacing, the new phase appearing in the form of helical nanofilaments.[7] Basically, a single HNF in the B4 phase looks like a rope of width $w \approx 35$ nm and half pitch $h \approx 130$ nm in which ≈5–8 smectic layers are twisted, a structure revealed in freeze-fracture and AFM imaging. In the bulk phase these basic units self-assemble parallel and next to one another to form oriented arrays in which the phase of the HNF twist is macroscopically coherent.

The growth of these filaments is controlled to some extent by the B2 layer texture and the LC interfaces. Thus, HNFs tend to grow with the filament axis P parallel to the air/LC interface, which enables their observation by AFM, in which the topographic relief associated with the rope-like surface of the individual filaments and the coherent twist combine to give a surface modulation with a periodicity of the HNF half pitch, evident in Figure 1c. In textures between glass slides the B2 forms planar-aligned birefringent textures with the smectic layers normal to the plates.[7] These remain in the B4 phase, but with little remnant birefringence.[15]

Figure 2–4 compare the results of cooling channel-confined NOBOW into the B4 with and without airflow. Without airflow the B2 grows in the channels in the form birefringent domains that are periodically modulated along the channel. This sort of modulated structure is found in calamitic smectics and the B7 phase of bent core molecules,[19,20] and generally arises from the frustration associated with the tendency for layer alignment parallel to the air/LC top interface and the alignment normal to the channel sides and bottom. Cooling channel-confined NOBOW into the B4 phase yields low birefringence domains (Figure 4). AFM imaging at room temperature shows the HNF orientation P at the air/LC interface

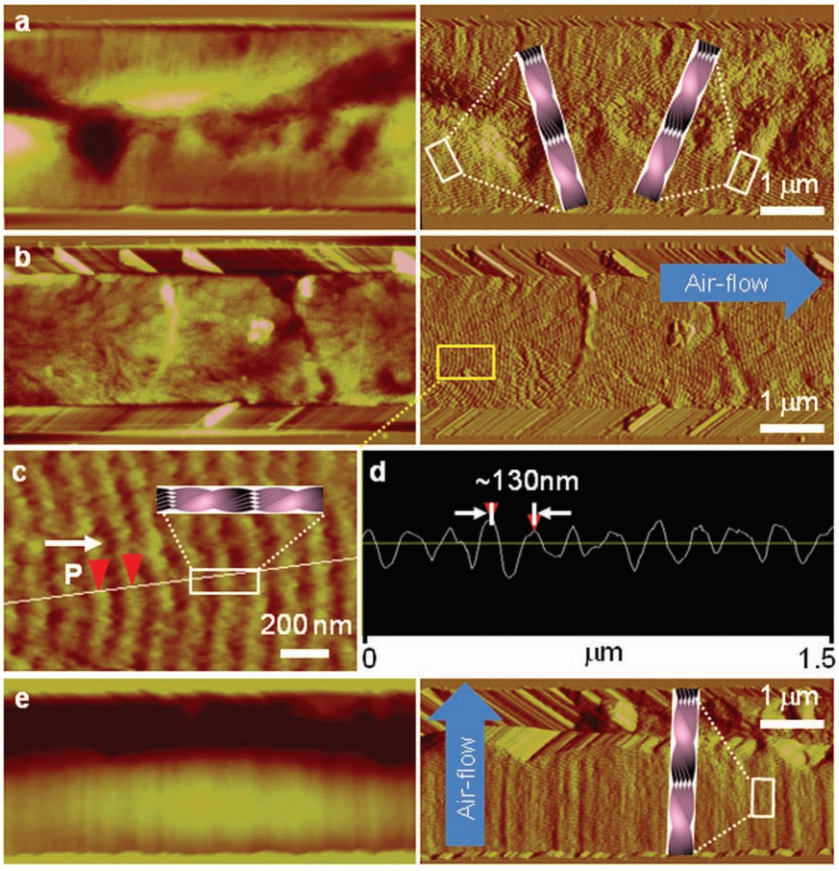

Figure 2. AFM images (left: height mode; right: deflection mode) of the B4 phase of NOBOW confined in channels and grown with and without air flow. a) Line patterns are aligned mostly along the channel direction although small parts of those are randomly oriented without applying the air flow. This means HNFs are mostly aligned perpendicular to the channels as shown in scheme. b) Uniformly aligned lines perpendicular to the channel can be seen after applying the air flow. This means HNFs are very well aligned along the direction of the channels and air flow. c) Enlarged area of (b) clearly shows half-pitch of HNFs. d) Surface profile of (c) shows the very periodic nanofilament helix of half-pitch, $h \approx 130$ nm. e) Perpendicularly aligned HNFs with few defects are shown when the air flow is applied perpendicular to the channel direction. The oblique lines at the top and bottom of the AFM images are due to the side of the tip sliding on the top edge of the channel wall.

tending to be nearly normal to the channel sidewalls, as shown in Figure 2. That is, the HNFs appear to have nucleated and grown out from the sidewalls.

For the air-flow experiments the hot stage temperature for obtaining the isotropic phase was set well above the bulk iso-B2 phase transition temperature $T = 175$ °C, to $T \approx 235$ °C at which the LC in the channels is isotropic, even in the presence of air flow. The gas flow sets up turbulent room temperature air above the sample surface, which tends to cool the air/sample interface by thermal conduction through a thin boundary layer. Since the thermal conductivity (λ) of the Si is much higher than that of the LC and air ($\lambda_{Si} \approx 148$ W m^{-1} °C^{-1}, $\lambda_{LC} \approx 0.2$ W m^{-1} °C^{-1}, and $\lambda_{air} \approx 0.025$ W m^{-1} °C^{-1}),[21] the temperature decrease of the LC surface due to the thermal flux out of the sample surface is much larger than that of the Si. In general, the heat flux $J = \lambda\left(\frac{\Delta T}{\Delta L}\right)$ will be out of the surface, where ΔT is the difference between the surface temperature and room temperature, and ΔL is the distance over which this temperature drop is achieved. With no air flow, taking $L \approx 1$ cm, one obtains $J \approx 400$ W m^{-2} and a temperature gradient in the LC at its surface of $\nabla T \approx 0.002$ °C μm^{-1}. With air flow one estimates a boundary layer thickness $\Delta L \approx 2$ μm and $\nabla T \approx 10$ °C μm^{-1}, and a LC surface temperature ≈50 °C cooler than the Si, with contours shown in Figure 3. The 2D simulation of the temperature distribution in the channel (Figure 3a) shows the lowest LC temperature along the LC centerline at the air/LC interface.

The factors relevant to the observed ordering of the HNFs are as follows:

(i) *Channel confinement*: The confining effect of the silicon channel makes the mesogenic units (bent-core molecules) align parallel with side wall and perpendicular to the bottom as shown in Figure 2. Near the LC/air interface the HNFs prefer to orient parallel to the surface[7] and the molecular anchoring parallel to the channel side wall induces, in absence of air flow, some HNF alignment in the LC/air interface plane upon cooling, with the HNFs generally normal to the side wall, as shown in Figure 2a and Figure S6, Supporting Information. As now discussed, the principal benefit of the channels is to provide a well-defined thermal gradient and LC flow orientation in the presence of air flow.

(ii) *Temperature gradients*: Without air flow the LC temperature in the channels is only a few 0.001 °C cooler along the channel centerline than at the channel surface, and no specific alignment effects have been attributable to this difference. However, with air flow, the ≈50 °C difference achieved means that with slow cooling the LC surface centerline will reach the I-B2, B2-B3, and B3-B4 transitions well before the LC that is closer to the Si, and these phases will then sequentially grow out from the centerline, toward from the channel surfaces. The importance of this air-flow-induced temperature gradient on the B4 HNF morphology was probed by cooling with the air flow on through the I–B2 transition and then turning the air flow off for the transition into the B4 phase. In this case the HNFs grow in from the channel walls (Figure S6, Supporting Information), as in the case where there was no air flow for either transition (Figure 2a). Thus, for air flow to affect the HNF alignment, it must be present when the B4 grows in.

(iii) *Shearing effect of air flow*: If the transition to the B4 is made in the presence of air flow, there is a significant change in the growth morphology, with AFM showing that the HNFs with air flow grow at the surface parallel to the air-flow direction (Figures 2b–e), as indicated by the distinctive $h = 130$ nm

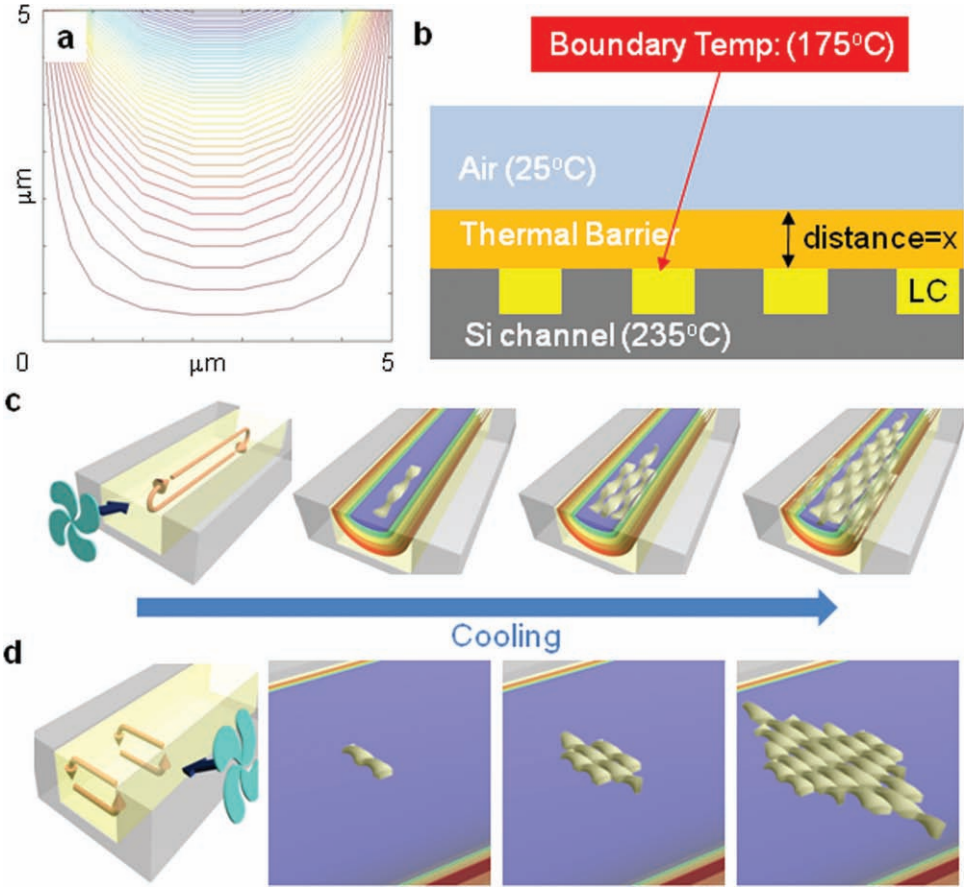

Figure 3. The 2D simulated temperature gradients in the channel and growing sequence with air flow. a) Temperature at the top-center surface of the LC is just under isotropic phase (≈175°C) and much warmer at the side and bottom walls of the silicon channel (≈235 °C), with a big thermal gradient (T = 60 °C). b) Scheme of the structure, thermal boundary layer, and LC. c) Serial perspective view of cooling with air flow along the channel showing temperature gradient from low *T* (blue) to high *T* (red), flow along the channel induced in the LC. and the resulting HNF growth, d) air flow applied to perpendicular to the channel direction produces LC circulation and therefore HNF orientation perpendicular to the channel.

topographic modulation of the HNF half pitch. Since the thermal distribution of the LC in the channels is largely the same for air flow parallel and normal to the channel, this observation points to the mechanical response of the LC system of the air flow as being the dominant alignment mechanism, rather than the direct thermal effects of the air flow. The thermal gradients associated with air flow do have the interesting consequence that the HNF $h = 130$ nm topographic modulation is much more robustly established at the surface, exhibiting clearer surface relief than for the no-air-flow case, likely a result of the of larger gradient in the air-flow case forcing the growth of HNFs to start at the surface. At high temperatures the HNFs can slide along one another, making the B4 phase fluid and shearable between flat plates. Because of the anisotropic shape of the HNFs, the HNF direction is oriented in shear flow parallel to the flow direction and normal to the flow gradient. This kind of shear alignment appears to be the operative alignment mechanism, with flow of the LC induced by the air. Such air-flow-induced LC velocity currents are indicated in Figure 3c,d for the two air-flow directions, the flow across the channel aligning the HNFs normal to the channel axis and the flow parallel to the channel inducing parallel orientation, respectively. The topographic patterning serves to hold the LC in place, enabling cellular flow. These closed flow velocity loops are present in the isotropic phase, influencing the orientation of the nucleating B4 domains as they appear along the channel centerline (Figures 2,3). This oriented growth penetrates down into the channel, as evidenced by high-resolution SEM imaging of fractured parts of air-flow-cooled samples, which show well-aligned HNFs in the interior of the channel as well as on the LC surface (Figures S7,S8, Supporting Information). This shear-induced HNF orientation, although preferable along the channel is not perfect, indicating that factors other than the induced flow come into play. HNFs appear by a nucleation and growth process that maintains their handedness over macroscopic distances, meaning that extant HNFs nucleate the new ones.[22] Such a process leads to an increase in the number of filaments growing in parallel and thereby to splay in $P(r)$, the spatial distribution of HNF directions (see the detail in Figure 3 of Ref. [7]). Splay of $P(r)$ would then lead to a bend in the surfaces of constant phase in the HNF twist and account for the bending of the modulation bands visible in the AFM images of the surface in Figure 2.

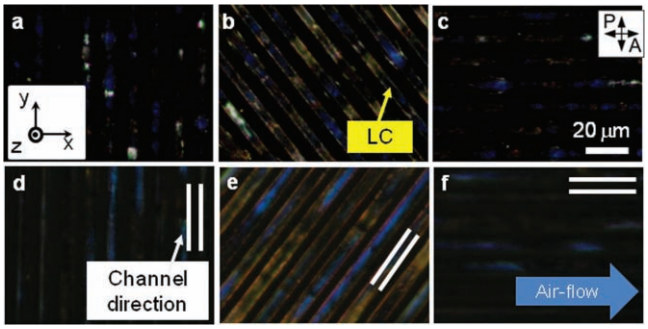

Figure 4. Comparison of depolarized transmission optical textures of the NOBOW B4 with and without air flow for several cell orientations. a,d,c,f) channels are parallel or normal to the polarizer. b,e) channels are at 45° to the polarizer. a–c) Without airflow the B4 shows mostly dark and bluish-to-yellowish domains in the channels. d–f) The textures with air flow are clearly smoother and exhibit channel lengths of several hundred nm with uniform birefringence, measurement of which yields $\Delta n \approx 0.04$ for the B4 phase.

The structure of the B4 phase in the channels either with or without air flow was also studied optically. DRLM images of NOBOW cooled in the channels without air flow show very dark grey and bluish optical morphology that are characteristics of B4 phase, with brightness that is increased when the crossed polarizer and analyzer are rotated to 45° relative to the channel direction (Figure 4a–c and Figure S9, Supporting Information), a result of weak birefringence due to the wall induced alignment (Figure 3a). Optical anisotropy is also found in B4 phase of NOBOW aligned by air flow (Figure 4d–f and Figure S10, Supporting Information), but with substantially larger birefringence, $\Delta n \approx 0.04$, comparable to that found in shear-aligned cells.[23] The independent AFM evidence of Figure 3b that the air flow treated B4 is well aligned in the channels thus shows that the B4 birefringence is actually quite small, a result of orientational averaging due to the molecular tilt and twist of the layers in the nanofilament structure (Figure 1b). The similarity of the $\Delta n \approx 0.04$ values found here for alignment in channels to that found in shear-aligned cells,[23] thus indicates that shearing cell plates can also substantially align the B4.

In summary, it was shown that topographic channel confinement can produce well-oriented domains of the helical nanofilaments of the B4 phase of several bent-core materials, but only if used in conjunction with air-flow-induced shear alignment. In this combination, the role of the topographic patterning of the surface is generalized beyond simply providing proximate aligning surfaces. The topography limits the gross flow of the LC, keeping it in the channels and controlling the LC circulation in the presence of the driving air flux. The topography combined with the high thermal conductivity of the confining patterned substrate controls where LC will first appear upon cooling. Thus, the success of this combination is based on the topography also controlling both temperature gradients and shear flow in the sample to be aligned. The achievement of alignment of the B4, notoriously difficult to orient with other methods, shows that the use of topographic confinement to control effects such as flow and gradients may prove to be a powerful combination in the use of LCs in applications beyond displays, where systems that are attractive are often difficult to align, for example in organic electronics.

Experimental Section

Sample Preparation: The bent-core molecule (NOBOW) was prepared as reported previously (Figure 1a).[15] Rectangular line and space patterned silicon wafers were prepared by using photolithography and reactive ion etching techniques.[18] The patterned surfaces employed here have a square cross section with a depth $d = 5$ μm, width $w = 5$ μm, and length $L = 10$ mm (Figure 1e) and were chemically cleaned for planar anchoring by immersion in a mixture of dimethylformamide (DMF) and methanol to remove both organic and inorganic impurities, followed by rinsing several times with deionized water. The LC material was dropped on one end of channels and filled by capillary force at the isotropic phase, using a hot stage (INSTEC HCS410) and controller (INSTEC STC 200), and then cooled very slowly down to room temperature at –0.02 °C min^{-1}. Samples were cooled either with or without air flow. During cooling samples with air flow, room temperature air was supplied by a 4-mm-inner-diameter copper tube, controlled by a flow regulator at a rate of 15 CFH (cubic feet per hour: ft^3 min^{-1}), 0.42 m^3 hr^{-1}, giving a velocity of flow about 9 m s^{-1} across the surface (Figure 1e).

Microscopy: The optical anisotropic textures of samples in the channels in the B4 phase were observed under DTLM and DRLM (Nikon Eclipse E400 POL) at room temperature. Study of the surface topology of the sample was performed under ambient conditions with an AFM (Nanoscope III: Veeco Instruments, Santa Barbara, CA). Contact mode AFM with Si_3N_4 cantilevers with a small spring constant of 0.06 N m^{-1} was used to minimize unexpected deformation of the sample. For SEM experiments, samples were imaged using JSM-7401F (JEOL) after coating with a 5-nm layer of gold to make the surface conductive and reduce electron beam damage.

Supporting Information

Supporting Information is available from the Wiley Online Library or from the author.

Acknowledgements

This work was supported by the MRSEC Program by NSF DMR-0820579, I2CAM Junior Exchange Award by NSF grant DMR-0645461 under ICAM-I2CAM. SEM experiments were carried out at NCF in CU-Boulder.

Received: December 6, 2010
Published online: March 24, 2011

[1] T. Niori, T. Sekine, J. Watanabe, T. Furukawa, H. Takezoe, *J. Mater. Chem.* **1996**, *6*, 1231.
[2] G. Pelzl, S.Diele, W. Weissflog, *Adv. Mater.* **1999**, *11*, 707.
[3] R. A. Reddy, C. Tschierske, *J. Mater. Chem.* **2006**, *16*, 907.
[4] D. R. Link, G. Natale, R.-F. Shao, J. E. Maclennan, N. A. Clark, E. Körblova, D. M. Walba, *Science* **1997**, *278*, 1924.
[5] D. A. Coleman, J. Fernsler, N. Chattham, M. Nakata, Y. Takanishi, E. Körblova, D. R. Link, R. -F. Shao, W. G. Jang, J. E. Maclennan, O. Mondainn-Monval, C. Boyer, W. Weissflog, G. Pelzl, L. -C. Chien, J. Zasadzinski, J. Watanabe, D. M. Walba, H. Takezoe, N. A. Clark, *Science* **2003**, *301*, 1204.
[6] L. E. Hough, M. Spannuth, M. Nakata, D. A. Coleman, C. D. Jones, G. Dantlgraber, C. Tschierske, J. Watanabe, E. Körblova, D. M. Walba, J. E. Maclennan, M. A. Glaser, N. A. Clark, *Science* **2009**, *325*, 452.
[7] L. E. Hough, H. -T. Jung, D. Krüerke, M. S. Heberling, M. Nakata, C. D. Jones, D. Chen, D. R. Link, J. Zasadzinski, G. Heppke,

J. P. Rabe, W. Stocker, E. Körblova, D. M. Walba, M. A. Glaser, N. A. Clark, *Science* **2009**, *325*, 456.
[8] S. R. Renn, T. C. Lubensky, *Phys. Rev. A* **1988**, *38*, 2132.
[9] H. Takezoe, Y. Takanishi, *Jpn. J. Appl. Phys.* **2006**, *45*, 597.
[10] C. W. Struijk, A. B. Sieval, J. E. J. Dakhorst, M. van Dijk, P. Kimkes, R. B. M. Koehorst, H. Donker, T. J. Schaafsma, S. J. Picken, A. M. van de Craats, J. M. Warman, H. Zuilhof, E. J. R. Sudhölter, *J. Am. Chem. Soc.* **2000**, *122*, 11057.
[11] T. D. Carson, W. Seo, S. -W. Tam-Chang, S. M. Casey, *Chem. Mater.* **2003**, *15*, 2292.
[12] R. J. Chesterfield, J. C. McKeen, C. R. Newman, P. C. Ewbank, D. A. da Silva Filho, J.-L. Bredas, L. L. Miller, K. R. Mann, C. D. Frisbie, *J. Phys. Chem. B* **2004**, *108*, 19281.
[13] V. G. Kozlov, G. Parthasarathy, P. E. Burrows, S. R. Forrest, Y. You, M. E. Thompson, *Appl. Phys. Lett.* **1998**, *72*, 144.
[14] L. Schmidt-Mende, A. Fechtenkötter, K. Müllen, E. Moons, R. D. Friend, J. D. MacKenzie, *Science* **2001**, *293*, 1119.
[15] T. Sekine, T. Niori, J. Watanabe, T. Furukawa, S. W. Choi, H. Takezoe, *J. Mater. Chem.* **1997**, *7*, 1307.
[16] C. Zhu, D. Chen, Y. Shen, C. D. Jones, M. A. Glaser, J. E. Maclennan, N. A. Clark, *Phys. Rev. E* **2010**, *81*, 011704.
[17] K. Takekoshi, K. Ema, H. Yao, Y. Takanishi, J. Watanabe, H. Takezoe, *Phys. Rev. Lett.* **2006**, *97*, 197801.
[18] D. K. Yoon, M. C. Choi, Y. H. Kim, M. W. Kim, O. D. Lavrentovich, H. -T. Jung, *Nat. Mater.* **2007**, *6*, 866.
[19] D. K. Yoon, J. Yoon, Y. H. Kim, M. C. Choi, J. Kim, O. Sakata, S. Kimura, M. W. Kim, I. I. Smalyukh, N. A. Clark, M. Ree, H. -T. Jung, *Phys. Rev. E* **2010**, *82*, 041705.
[20] D. K. Yoon, R. Deb, D. Chen, E. Körblova, R. -F Shao, K. Ishikawa, N. V. S. Rao, D. M. Walba, I. I. Smalyukh, N. A. Clark, *Proc. Natl. Acad. Sci. USA* **2010**, *107*, 21311.
[21] Y. S. Touloukian, *Thermophysical Properties of Matter*, Springer, New York **1970**.
[22] D. Chen, C. Zhu, R. K. Shoemaker, E. Körblova, D. M. Walba, M. A. Glaser, J. E. Maclennan, N. A. Clark, *Langmuir* **2010**, *26*, 15541.
[23] A. Rastegar, H. Wulterkens, H. Verscharen, T. Rasing, G. Heppke, *Rev. Sci. Inst.* **2000**, *71*, *4492*.